

Article

Cylindrical Resonator Utilizing a Curved Resonant Grating as a Cavity Wall

Yasuo Ohtera *, Shohei Iijima and Hirohito Yamada

Graduate School of Engineering, Tohoku University, Aramaki-Aza-Aoba 6-6, Aoba-ku, Sendai, Miyagi 980-8579, Japan; E-Mails: iijima@ecei.tohoku.ac.jp (S.I.); yamada@ecei.tohoku.ac.jp (H.Y.)

* Author to whom correspondence should be addressed; E-Mail: ohtera@ecei.tohoku.ac.jp;
Tel./Fax: +81-22-795-7103.

Received: 26 December 2011; in revised form: 15 February 2012 / Accepted: 17 February 2012 /
Published: 27 February 2012

Abstract: A thin-film grating on a curved substrate functions as a highly reflective and wavelength sensitive mirror for a diverging wave that has the same curvature as the substrate. In this paper we propose a cylindrical cavity surrounded by a curved resonant grating wall, and describe its resonance characteristics. Through finite-difference time-domain (FDTD) simulation we have clarified that this type of cavity supports two resonance modes: one is confined by Fresnel reflection and the other by resonance reflection of the wall. We have also demonstrated that the latter mode exhibits a Q factor several orders of magnitude higher than that of the former mode.

Keywords: resonant grating; guided-mode resonance; cylindrical cavity; circular cavity

1. Introduction

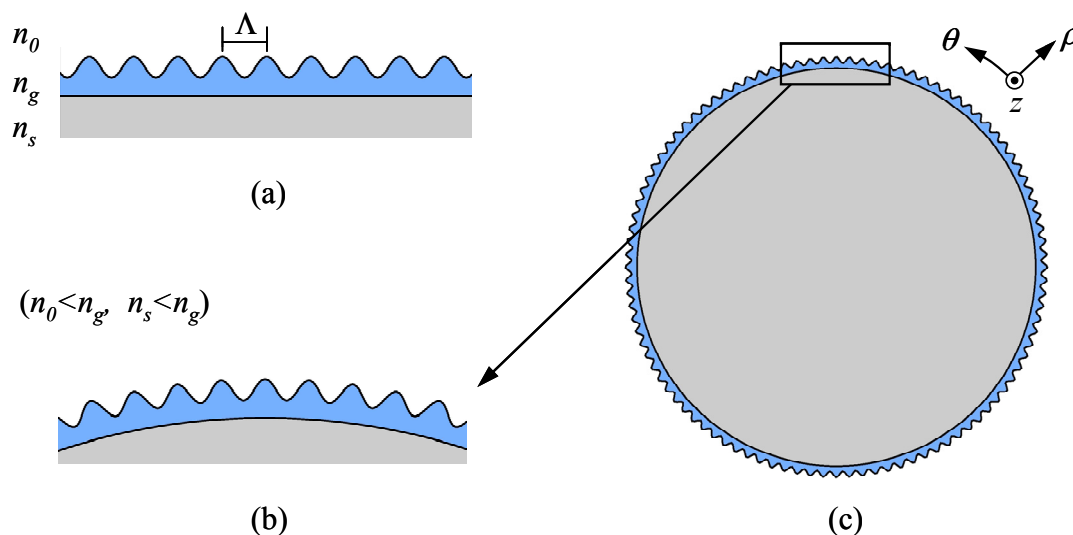
The cylindrical cavity is one of the most fundamental types of resonant cavities, and has been used to construct, for example, wavelength filters for microwaves [1,2], millimeter waves [3,4] and Terahertz waves [5]. The cylindrical cavity also has a number of important applications in the lightwave field, such as couplers and laser cavities [6–8].

Similar to other types of resonators, the quality factor (Q) of a cylindrical cavity, which is a basic characteristic, depends on the performance of the cavity walls. External Q increases with wall reflectivity, provided that the wall is lossless. The full width at half maximum (FWHM) of the resonance peak becomes narrow, while the free spectral range (FSR) widens as the cavity radius

increases. This dependence is the same as conventional Fabry-Perot etalons which utilize a pair of flat mirrors. Various trials have been conducted in recent years aiming to control the resonance characteristics of circular cavities. One of the most straightforward approaches is to add sub-wavelength scale index perturbation to the walls. For example, the application of periodic index modulation along the radial [9,10] and azimuthal [11] directions has been found to be effective for selecting the specific order of resonance modes.

Guided-mode resonance (GMR) is another useful phenomenon for controlling the reflection spectrum at material boundaries [12,13]. The main structure for GMR is a thin-film grating surrounded by relatively low-index materials. GMR occurs as a result of resonant coupling between an externally incident plane wave and a leaky guiding mode supported by the grating film as a periodic slab waveguide [14]. Coupled leaky mode propagates inside the slab and is again diffracted by the grating, and radiated out of the film. Theoretically, the reflectivity for plane wave incidence is as high as 100% at the wavelength and angle of incidence where all of the radiated waves interfere constructively [15]. Thin-film gratings are therefore often called Resonant Gratings (RG) or Resonant Sub-wavelength Gratings (RSG) [16,17]. A RG functions basically as a wavelength selective mirror, and its reflection spectrum can be tailored by designing the periodic structure appropriately [18]. Highly efficient reflection [19], as well as the ability to tailor the spatial beam profile, has been successfully demonstrated [20].

Figure 1. Schematic view of part of a flat/curved resonant grating and a circular cavity. (a) Conventional thin-film grating with a sinusoidal profile on a flat substrate; (b) Curved structure; (c) Cylindrical cavity with a curved grating wall.



Recently, attempts have been made to extend the GMR concept to curved substrate structures [21,22]. We have shown that RGs with constant local curvature exhibit similar resonant reflection for concentric circular waves [21]. Based on the insights obtained, in this paper we propose a novel cylindrical resonator surrounded by a curved RG wall. Our sample structure is based on the conventional thin-film surface grating with a sinusoidal cross-sectional profile as shown in Figure 1. Some of the fundamental characteristics, such as resonance wavelength, Q factor, and modal fields are calculated by numerical simulation. It is also shown that the resonator supports extremely high-Q

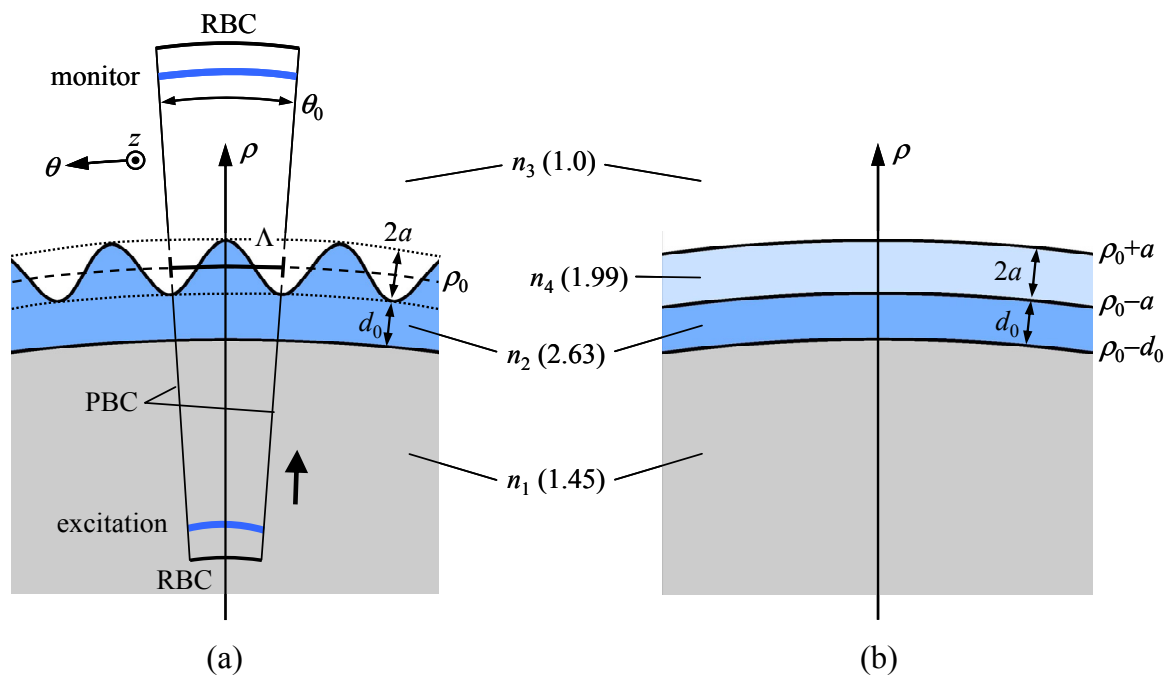
modes compared to conventional dielectric circular resonators. Note that the major difference between the proposed structure and the microgear disk resonator [11] is the refractive index inside the cavity. In our structure it is essential to make the index lower than that of the constituent material of the RG wall, in order to confine the light field inside the cavity by the effect of GMR. The resonant modes of the cavity to be confined thus have zero-th azimuthal order.

2. Characteristics of a Curved RG

2.1. Structure and Method of Calculation

Before calculating the characteristics of the cavity, we first analyzed the reflection property of the wall part. A schematic diagram of the structure is shown in Figure 2(a). One of our future targets is to design three-dimensional structures like a micro-disk resonator on a planar integrated light circuit. However, in this study, we simplified the structure as a two-dimensional one using the effective index method [23], to identify the main resonance characteristics of the curved RG-type resonator. Refractive index and electromagnetic fields were assumed to be uniform in the z (normal to the paper) direction of the figure. Throughout this paper we consider only TM modes (E_z , H_θ , and H_ρ).

Figure 2. Detail of the sample structures. (a) Curved resonant grating (proposed structure). ρ_0 , $2a$ and d_0 are the average radial position, depth and base thickness of the grating, respectively. The region surrounded by a solid line indicates the computational domain for FDTD. PBC and RBC stand for Periodic and Radiation Boundary Conditions, respectively; (b) Reference curved slab structure. The grating region is replaced by an average refractive index layer.



Let the distance between the center of curvature and the average height of the grating be ρ_0 . The depth and average thickness of the grating layer are $2a$ and d_0 , respectively. The index of the grating layer, $n_2 = 2.63$, is set close to the effective index of the fundamental TM mode of the InP/air disk

structure [24]. The refractive indexes of the inner and outer spaces are $n_1 = 1.45$ and $n_3 = 1.0$, respectively. The local thickness of the grating layer, $d(\theta)$, is defined as:

$$d(\theta) = d_0 + a\{1 + \cos(2\pi\theta/\theta_0)\} \tag{1}$$

where $d_0 = 0.68\Lambda$ and $a = 0.25\Lambda$.

These parameters were determined so that the lowest-order GMR wavelength is in the valley region of the reflection spectrum (spectra are shown in Figure 3).

The angle θ_0 denotes the azimuthal extent of a unit grating, and is expressed as $\theta_0 = 2\pi/m$ [rad] where m is the total number of gratings on a wall edge. The pitch of the grating, Λ , is defined as the length of an arc at the average grating height, $\Lambda = \rho_0\theta_0$.

Figure 3. Reflection spectra viewed from inside the curved grating. “ m ” is the number of gratings on the outer edge of the cavity wall. The broken line shows the spectrum of the average index structure of Figure 2(b) for $m = 50$.

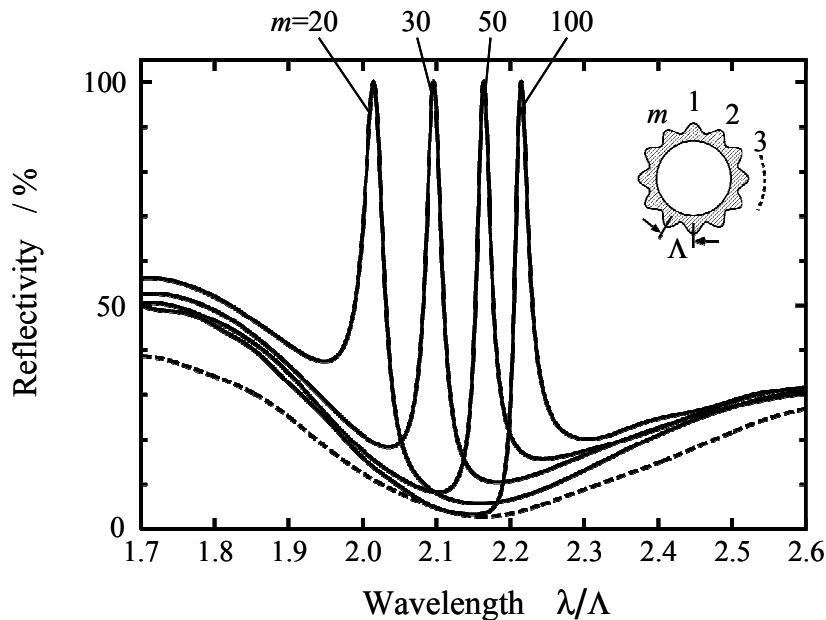


Figure 2(b) shows a simple cylindrical structure where the grating region is replaced by a mean refractive index layer. This structure was also analyzed to see the resonance characteristics where the grating does not exhibit GMR. The average index of the replaced region, n_4 , is defined as:

$$n_4 = \sqrt{\frac{n_2^2 + n_3^2}{2}} \approx 1.99 \tag{2}$$

The reflectivity for a cylindrical wave launched from inside the curvature ($\rho < \rho_0 - d_0$) is calculated by a cylindrical coordinate version of the two-dimensional FDTD method [25]. The computational domain is surrounded by a solid line in Figure 2(a). The angular direction is limited by one grating period. Both sides are connected by periodic boundary conditions (PBCs). The radial ends are terminated by radiation boundary conditions (RBCs) [26] to absorb inward converging and outward diverging waves.

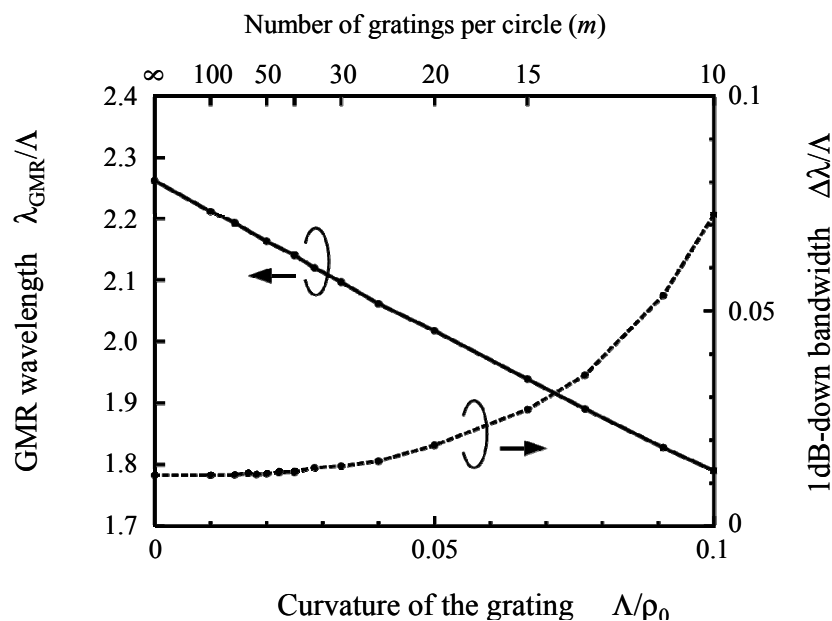
2.2. Reflection Spectra

A concentric cylindrical wave of a center wavelength of $\lambda_0 = 2\Lambda$ with a temporal Gaussian envelope was excited near the inner RBC. Because there is insufficient space between the excitation position and the inner surface of the RG, it is difficult to temporally separate the excited and reflected waves. Therefore we tried to estimate the reflectivity using the waveform monitored outside the RG. The recorded time-domain waveform of E_z and H_θ are Fourier transformed and then multiplied to obtain the radial component of the Poynting vector, $P_\rho(\lambda)$. A similar calculation is carried out for a uniform space of $n = 1.45$ to obtain a reference Poynting vector $P_{\rho 0}(\lambda)$. The reflectivity of RG is then evaluated by $R(\lambda) = 1 - P_\rho(\lambda)/P_{\rho 0}(\lambda)$. The results for various curvature radii are plotted in Figure 3. It is clearly seen that the spectra are the superposition of average structure reflectivity (Figure 2(b)) and a sharp resonance peak.

The relationships between GMR wavelength, bandwidth and curvature are summarized in Figure 4, which shows that the resonance wavelength depends almost linearly on the curvature. This can be explained as follows: the modal field of a curved waveguide shifts to the outer side as the curvature increases [27]. In the structure of Figure 2(a), the average refractive index outside the grating layer is low, and so the mean optical path length for the guided mode becomes small as the curvature increases. This tends to shorten the resonance wavelength.

We also confirmed that the peak reflectivity at the GMR wavelength remains at almost 100% for structures with $m > 20$.

Figure 4. Relationships between the curvature of the grating, GMR wavelength and 1-dB bandwidth.



2.3. Effective High-Index Mirror Position

As we will show in the next section, resonance wavelengths of a RG-type cylindrical cavity exhibit strange behavior near the GMR wavelength of the RG wall. We thought that the key physics behind

such behavior would be a rapid phase shift of the RG upon reflection. Because the phase of the reflection is directly connected with the effective reflection plane where the field amplitude becomes either minimum or maximum, it is convenient to regard RGs as a uniform medium with an effective reflection position. By substituting an effective cavity radius, which is a summation of the nominal cavity radius and the penetration depth of the effective reflection plane, into the equation for the conventional resonance condition, we will be able to obtain resonance wavelengths for the curved RG-type cavity. Also, through such calculation we will be able to explain the strange behavior of the resonance wavelength of the cavity. Note that outside GMR, the RG shows finite transmission. Therefore it is more reasonable to regard the RG as a high-index or low-index medium rather than a metallic mirror. The principle of calculating the effective reflection positions of curved RGs as a high-index medium is as follows.

The electric field inside the curvature can be well approximated as a superposition of diverging and converging waves as follows, except for the region very close to the grating layer:

$$E_z(n_1k_0\rho) = A_c H_0^{(1)}(n_1k_0\rho) + A_d H_0^{(2)}(n_1k_0\rho) \quad (\rho < \rho_0 - d_0) \quad (3)$$

where $H_0^{(1)}$ and $H_0^{(2)}$ denote the 0th-order Hankel function of the first and second kind, and correspond to converging and diverging waves, respectively. A_c and A_d are their complex amplitudes. k_0 and ρ are the free space wave number and the radial coordinate, respectively.

We define the effective mirror plane as the radial position beyond which the space can be regarded as an infinitely extending high-index medium. The amplitude reflectivity of the electric field on such a plane ($\rho = \rho_{eff}$) should therefore be a negative real number. The electric field at such a plane can thus be expressed as:

$$E_z(n_1k_0\rho_{eff}) = AH_0^{(2)}(n_1k_0\rho_{eff})(1 - |r|) \quad (4)$$

where A and $|r|$ are another complex amplitude and the norm of the amplitude reflectance, respectively. Considering Equation (3), the field inside the curvature can be expressed as follows.

$$E_z(n_1k_0\rho) = A_d \left\{ H_0^{(2)}(n_1k_0\rho) - |r| \frac{H_0^{(2)}(n_1k_0\rho_{eff})}{H_0^{(1)}(n_1k_0\rho_{eff})} H_0^{(1)}(n_1k_0\rho) \right\} \quad (\rho < \rho_0 - d_0) \quad (5)$$

Amplitude factors can be expressed using Equations (3) to (5) as follows:

$$A = A_d, \quad \frac{A_c}{A_d} = -|r| \frac{H_0^{(2)}(n_1k_0\rho_{eff})}{H_0^{(1)}(n_1k_0\rho_{eff})} \quad (6)$$

We tried to calculate the relationship between the wavelength and the effective mirror position (ρ_{eff}). First, we calculated the field distribution at a wavelength of interest using the FDTD method. An example for the $m = 50$ structure is shown by the solid line in Figure 5. Then the data of $\rho/\Lambda < 6$ was least-squares fitted to Equation (3) to obtain A_c and A_d . The fitted field is shown by the dotted line in the figure. Finally, $|r|$ and ρ_{eff} were calculated using Equation (6). The inset of Figure 5 is a magnified view of the fitted field near the grating layer. The calculated relationships between wavelength and effective mirror position for RGs and average index structures are summarized in Figure 6. This result

clarifies that the mirror positions for both structures behave similarly far from the GMR wavelength. For the average layer structure, as the wavelength moves across the minimum reflection point, the mirror position slowly shifts by about a quarter wavelength; this phenomenon can be commonly seen in a flat dielectric film. On the other hand, for a curved RG this shift is more abrupt: the mirror position appears almost to jump at the GMR wavelength. This can be interpreted to mean that the complex reflectivity of the RG follows a sharp Lorentzian function near the resonance wavelength as described by Fan *et al.* [28].

Figure 5. Example of a calculated field intensity profile upon reflection (solid line) and its extrapolated curve (dotted line), for the $m = 50$ structure. The latter is a linear summation of $H_0^{(1)}(n_1k_0\rho)$ and $H_0^{(2)}(n_1k_0\rho)$.

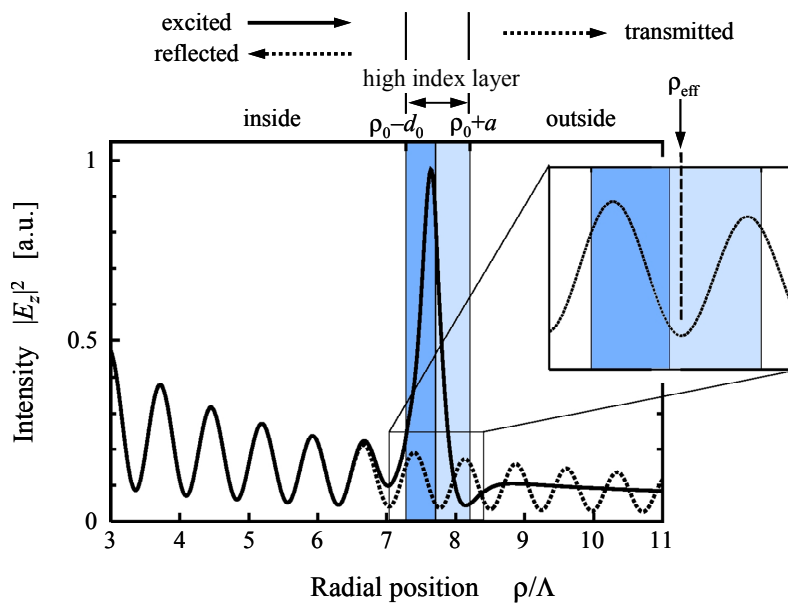
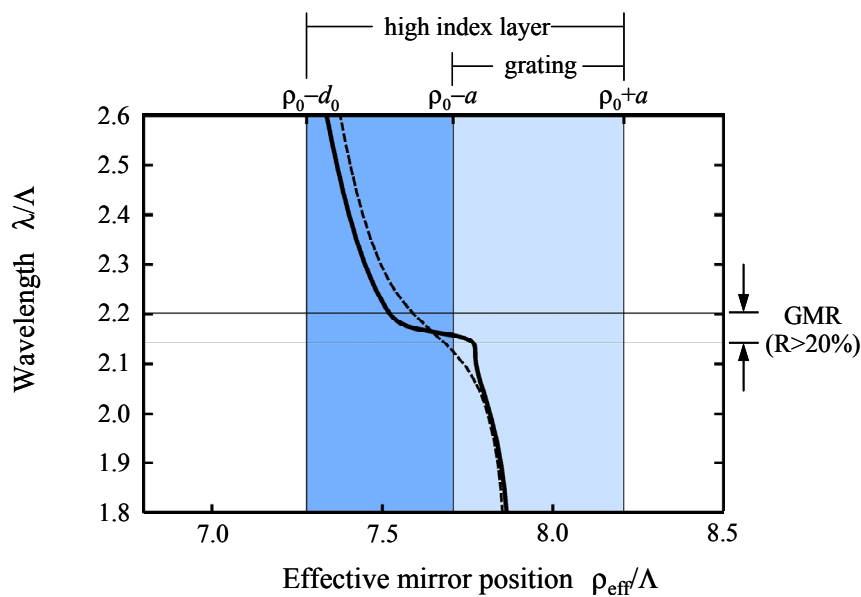


Figure 6. Estimated effective high-index mirror positions, for the $m = 50$ structure. Solid and dashed lines are curved RG and average index slab, respectively.



3. Characteristics of RGC

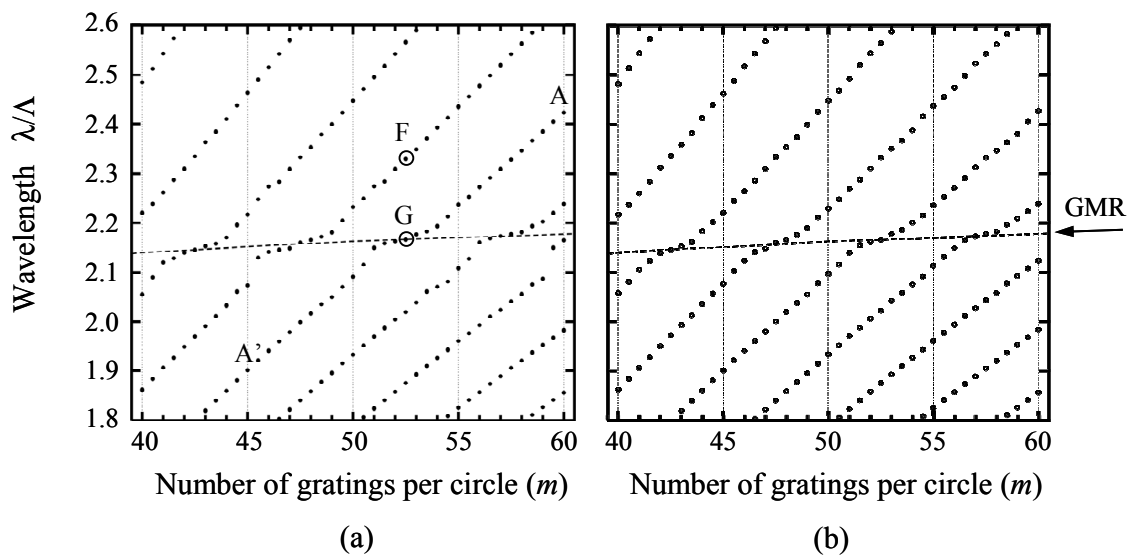
3.1. Resonance Wavelength of the Cavity Mode

The relationships between the structural parameters of the cavity (such as radius and refractive index) and the resonance wavelength are fundamental information for the resonator. We calculated the resonance wavelengths of cylindrical cavities surrounded by the RG walls with various curvature radii. The domain for FDTD simulation was extended to the center of the cavity.

We placed a point excitation source E_z at the center, and monitored the electromagnetic fields at two pitches outside the grating ($\rho = \rho_0 + 2\Lambda$). Peak wavelengths contained in the monitored waveform were extracted using Fast Fourier Transformation (FFT). These wavelengths correspond to the resonance wavelengths of the cavity system.

The above calculation was carried out for various cavity radii, and the results are plotted as a function of m in Figure 7(a). This figure shows that there are roughly two kinds of resonance series: (a) an almost linear series extending from the top right to bottom left; and (b) A wavy series located around $2.1 < \lambda/\Lambda < 2.2$. The former is the resonance modes where RG almost serves as a mean dielectric structure as in Figure 2(b). The resonance wavelength and Q are determined by the Fresnel reflection constant of the multilayer, so we call these modes “Fresnel modes” hereafter. The latter series are dependent on the GMR spectrum of the RG, and we call them “Grating modes” for convenience.

Figure 7. Calculated resonance wavelengths for various cavity sizes. The dashed line indicates the GMR wavelength of the curved RG wall. (a) Determined from the peaks of radiation spectra monitored outside the cavity; (b) Estimated by $J_0(n_1k_0\rho_{eff})=0$, where ρ_{eff} is the radial position of the effective high-index mirror.



The resonance condition for TM modes of a hollow circular metallic cavity is given as zeros of a Bessel function as follows [29]:

$$J_0(n_1k_0\rho_c) = 0 \tag{7}$$

where ρ_c is the radius of the cavity. We tried to check whether or not this condition also applies to our RG-type resonator. We replaced the physical radius (ρ_c) by the effective one (ρ_{eff}) and plotted the wavelengths which satisfy the above relationship for various cavity sizes (m). The effective position, ρ_{eff} , for various curvatures was calculated by the procedure described in Section 2.3. The result is shown in Figure 7(b). These results look similar for both Fresnel and Grating modes. It is clear that the deformation of the resonance curve near the GMR wavelength corresponds to the behavior of ρ_{eff} seen in Figure 6. This indicates that the resonance wavelength of the proposed cavity is also governed by the conventional resonance condition of Equation (7), regardless of the confinement mechanism (Fresnel reflection or resonant reflection) of the modes.

3.2. Quality Factor

Next, Q-factors of the resonance series marked by A-A' in Figure 7(a) are evaluated using the following equation [30]:

$$Q = \frac{\omega_0 \tau_0}{2} \tag{8}$$

where ω_0 and τ_0 are the angular frequency and the decay time, respectively. The results are plotted as filled circles in Figure 8. Practically, the total number of gratings on the cavity wall (m) must be an integer number. However, according to our FDTD method, non-integer m can be handled without difficulty, because we need to specify only the azimuthal extent (θ_0) of the unit grating. In Figure 8, the results for non-integer m structures are also plotted as a dotted line.

Figure 8. Quality factor of the resonance series indicated by A-A' in Figure 7(a).

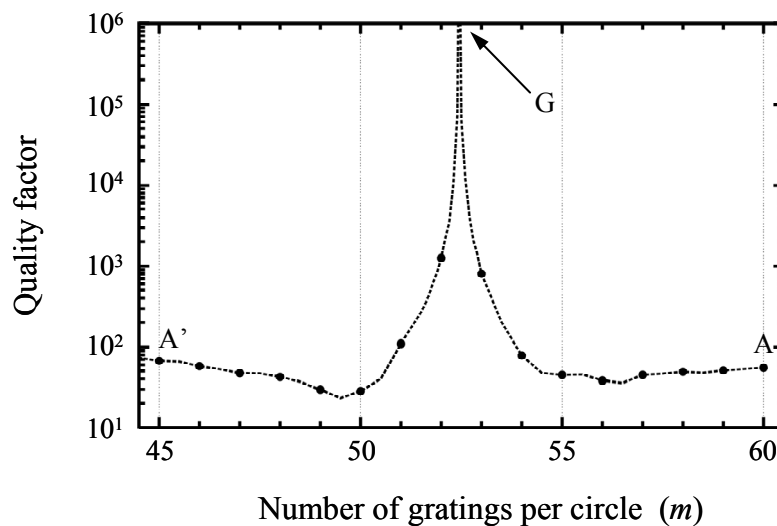
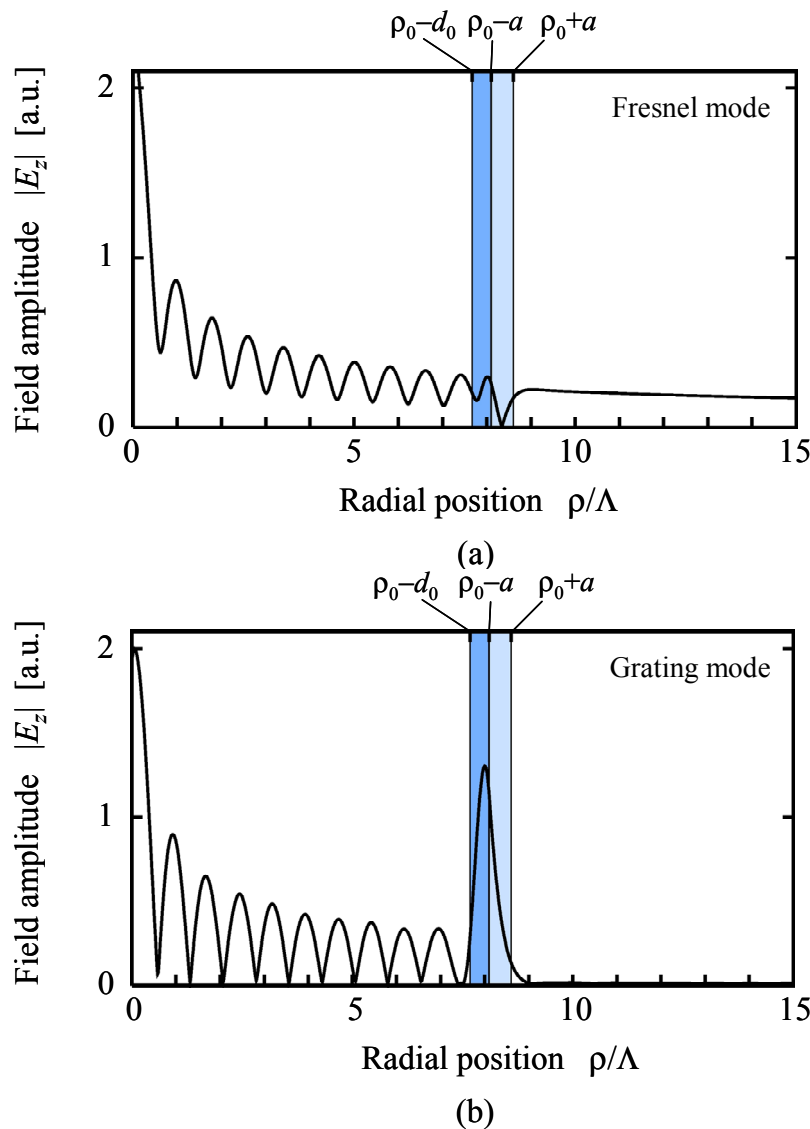


Figure 8 shows that Q of the grating mode ($52 < m < 53$) becomes extremely high, corresponding to the high reflectivity of the RG wall. Q of other Fresnel modes is less than 100. In other words, only one high-Q resonant mode exists in a wide range of wavelength, which means that this RG type cavity effectively behaves as a single-mode resonator.

Electric field distributions of a Fresnel mode (point “F” in Figure 7) and high-Q grating mode (point “G” in Figures 7 and 8) are displayed in Figure 9(a,b), respectively. In Figure 9(a), the standing wave

ratio (SWR) inside the cavity looks small due to the low reflectivity of the cavity wall. The wavelength is far from GMR, and therefore the field intensity in the grating layer is of the same order as that inside the cavity. In addition, substantial field leakage is seen outside. On the contrary, in Figure 9(b) the field intensity in the grating layer is enhanced due to the guided mode resonance. This characteristic is well known for RGs [31]. Also, the high reflectivity of the wall keeps the SWR almost at infinity. There is almost no field leakage outside the cavity.

Figure 9. (a) Electric field distribution of a Fresnel mode, indicated by “F” in Figure 7(a); (b) High-Q grating mode, indicated by “G” in Figure 7(a) and Figure 8. The size of the cavity is $m = 52.47$ (virtual structure).



As we showed in Figure 3, the basic characteristics of our curved RG mirror are similar to those of the conventional flat RG, and so the tolerance to changes in various structural or material parameters will be approximately the same. The cavity characteristics (tolerance for achieving high-Q) will also have a similar level of tolerance.

4. Conclusions

We clarified the resonance characteristics of cylindrical resonant cavities surrounded by a curved grating wall through numerical simulation. The cavity was found to support two kinds of resonant modes, whose Q are determined by the Fresnel and GMR reflection constant at the cavity/wall boundary, respectively. We also showed that, in the example structure, the quality factor of the latter modes can be increased by several orders of magnitude compared with the former modes. The proposed cavity was found to function as a large-area, effectively single-mode cavity. This type of structure will be a useful platform for realizing micro-photonic devices such as single-mode lasers, high-finesse wavelength filters and biosensors. Having clarified the fundamental characteristics, we will investigate as our next study the optimum structural design which is more robust against fabrication errors of size, shape, and refractive index.

Acknowledgment

This research was in part supported by KAKENHI, Grant-in-Aid for Scientific Research (B) 23360145 of Japan Society for the Promotion of Science (JSPS).

References

1. Collin, R.E. Electromagnetic Resonators. In *Foundations for Microwave Engineering*, 2nd ed.; Wiley: Hoboken, NJ, USA, 2001; pp. 496–517.
2. Cohn, S.B. Microwave bandpass filters containing high-Q dielectric resonators. *IEEE Trans. Microw. Theory Tech.* **1968**, *MTT-16*, 218–227.
3. Jiao, X.H.; Cuillon, P.; Bermudez, L.A.; Auxemery, P. Whispering-Gallery modes of dielectric structures: Applications to millimeter-wave bandstop filters. *IEEE Trans. Microw. Theory Tech.* **1987**, *MTT-35*, 1169–1175.
4. Cros, D.; Guillon, P. Whispering Gallery dielectric resonator modes for W-band devices. *IEEE Trans. Microw. Theory Tech.* **1990**, *38*, 1667–1674.
5. Preu, S.; Schwefel, H.G.L.; Malzer, S.; Dohler, G.H.; Wang, L.J.; Hanson, M.; Zimmerman, J.D.; Gossard, A.C. Coupled whispering gallery mode resonators in Terahertz frequency range. *Opt. Express* **2008**, *16*, 7336–7343.
6. Alexopoulos, N.G.; Kerner, S. Coupled power theorem and orthogonality relations for optical disk waveguides. *J. Opt. Soc. Am.* **1977**, *67*, 1634–1638.
7. Vahala, K.J. Optical microcavities. *Nature* **2003**, *424*, 839–846.
8. Ilchenko, V.S.; Matsko, A.B. Optical resonators with whispering-gallery modes-part II: Applications. *IEEE J. Sel. Top. Quantum Electron.* **2006**, *12*, 15–32.
9. Scheuer, J.; Yariv, A. Annular Bragg defect mode resonators. *J. Opt. Soc. Am. B* **2003**, *20*, 2285–2291.
10. Sun, X.; Yariv, A. Surface-emitting circular DFB, disk-, and ring-Bragg resonator laser with chirped gratings: A unified theory and comparative study. *Opt. Express* **2008**, *16*, 9155–9164.
11. Fujita, M.; Baba, T. Microgear laser. *Appl. Phys. Lett.* **2002**, *80*, 2051–2053.

12. Wang, S.S.; Magnusson, R.; Bagby, J.S.; Moharam, M.G. Guided-mode resonances in planar dielectric-layer diffraction gratings. *J. Opt. Soc. Am. A* **1990**, *7*, 1470–1474.
13. Wang, S.S.; Magnusson, R. Theory and applications of guided-mode resonance filters. *Appl. Opt.* **1993**, *32*, 2606–2613.
14. Vincent, P.; Neviere, M. Corrugated dielectric waveguides: A numerical study of the second-order stop bands. *Appl. Phys.* **1979**, *20*, 345–351.
15. Rosenblatt, D.; Sharon, A.; Friesem, A.A. Resonant grating waveguide structures. *IEEE J. Quantum Electron.* **1997**, *33*, 2038–2059.
16. Peters, D.W.; Kemme, S.A.; Hadley, G.R. Effect of finite grating, waveguide width, and end-facet geometry on resonant subwavelength grating reflectivity. *J. Opt. Soc. Am. A* **2004**, *21*, 981–987.
17. Peters, D.W.; Boye, R.R.; Wendt, J.R.; Kellogg, R.A.; Kemme, S.A.; Carter, T.R.; Samora, S. Demonstration of polarization-independent resonant subwavelength grating filter arrays. *Opt. Lett.* **2010**, *35*, 3201–3203.
18. Ding, Y.; Magnusson, R. Resonant leaky-mode spectral-band engineering and device applications. *Opt. Express* **2004**, *12*, 5661–5674.
19. Liu, Z.S.; Tibuleac, S.; Shin, D.; Young, P.P.; Magnusson, R. High-efficiency guided-mode resonance filter. *Opt. Lett.* **1998**, *23*, 1556–1558.
20. Fattal, D.; Li, J.; Peng, Z.; Fiorentino, M.; Beausoleil, R. G. Flat dielectric grating reflectors with focusing abilities. *Nature Photon.* **2010**, *4*, 466–470.
21. Ohtera, Y.; Iijima, S.; Yamada, H. Guided-mode resonance in curved grating structures. *Opt. Lett.* **2011**, *36*, 1689–1691.
22. Lu, M.; Zhai, H.; Magnusson, R. Focusing light with curved guided-mode resonance reflectors. *Micromachines* **2011**, *2*, 150–156.
23. Hocker, G.B.; Burns, W.K. Mode dispersion in diffused channel waveguides by the effective index method. *Appl. Opt.* **1977**, *16*, 113–118.
24. Huy, K.P.; Morand, A.; Amans, D.; Benech, P. Analytical study of the whispering-gallery mode in two-dimensional microgear cavity using coupled-mode theory. *J. Opt. Soc. Am. B* **2005**, *22*, 1793–1803.
25. Taflove, A. *Computational Electrodynamics: The Finite-Difference Time-Domain Method*; Artech House: Boston, MA, USA, 1995; pp. 397–410.
26. Xu, Y.; Vuckovic, J.S.; Lee, R.K.; Painter, O.J.; Scherer, A.; Yariv, A. Finite-difference time-domain calculation of spontaneous emission lifetime in a microcavity. *J. Opt. Soc. Am. B* **1999**, *16*, 465–474.
27. Gambling, W.A.; Matsumura, H.; Ragdale, C.M. Field deformation in a curved single-mode fibre. *Electron. Lett.* **1978**, *14*, 130–132.
28. Fan, S.; Joannopoulos, J.D. Analysis of guided resonances in photonic crystal slabs. *Phys. Rev. B* **2002**, *65*, 235112:1–235112:8.
29. Pozer, D.M. *Microwave Engineering*, 3rd ed.; Wiley: Hoboken, NJ, USA, 2005; pp. 117–126.
30. Haus, H.A. *Waves and Fields in Optoelectronics*; Prentice-Hall: Upper Saddle River, NJ, USA, 1984; p. 208.

31. Magnusson, R.; S-Saremi, M. Widely tunable guided-mode resonance nanoelectromechanical RGB pixels. *Opt. Express* **2007**, *15*, 10903–10910.

© 2012 by the authors; licensee MDPI, Basel, Switzerland. This article is an open access article distributed under the terms and conditions of the Creative Commons Attribution license (<http://creativecommons.org/licenses/by/3.0/>).